Residual stresses in Selective Laser Sintering and Selective Laser Melting

Peter Mercelis - Jean-Pierre Kruth
Dept. Of Mechanical Engineering - division PMA
University of Leuven

Reviewed, accepted August 24, 2005

Abstract

This paper presents an investigation into residual stresses in Selective Laser Sintering and Selective Laser Melting. First, the origin of these stresses is explored, and a simple theoretical model is presented to predict the residual stress distribution. Next, an experimental model is developed, which can be used to measure the actual residual stresses remaining in the parts produced. A set of test samples is then tested to investigate the influence of the process parameters on the residual stresses being developed. At last, some methods to reduce the residual stress are presented

Introduction

Selective Laser Sintering and Selective Laser Melting are two production technologies offering great advantages and opportunities compared to traditional material removal techniques [1],[2]. However, the residual stresses that arise in the parts being produced impose some serious limitations to the practical use, since they introduce part deformations and/or micro cracks. Moreover, large residual stresses can limit the load resistance of the parts compared to a stress free state.

In order to investigate the residual stresses, the origin of the stresses is firstly explained. Next, a simple theoretical model is presented to predict the basic residual stress distribution. Using an experimental procedure, residual stress profiles are then measured in a set of test samples having different kinds of process parameters. Thus, the effect of the process parameters on the residual stress can be concluded. Finally, some guidelines are presented to reduce the residual stress in Selective Laser Sintering and Selective Laser Melting.

The difference between Selective Laser Sintering and Selective Laser Melting concerns the binding mechanism that occurs between the powder particles [2]. In Selective Laser Sintering, either a combination of a low melting binder and high melting structural material is used - called Liquid Phase Sintering (LPS) - or the powder particles are just partially molten. In case of LPS, a post treatment is generally necessary to enhance the mechanical properties and to increase the part's density. In Selective Laser Melting, the powder particles are fully molten. Since the border between SLS and SLM is rather vague, the stress inducing mechanisms are explained generally for the case of Selective

Laser Melting. In the case of partial melting without infiltration, the same stress inducing mechanisms will occur. On the other hand, in the case of the LPS mechanism, the furnace cycle that is used to infiltrate the parts, will also result in stress relaxation, so the resulting parts can be expected to be stress free.

The origin of residual stresses

Residual stresses are stresses that remain inside a material, when it has reached equilibrium with its environment. Residual stresses are generally classified according the scale at which they occur [3]. This investigation includes only type I residual stresses, which vary over large distances, namely the dimensions of the part. These macro stresses can result in large deformations of the part. Type II and type III residual stresses, which occur due to different phases in the material and due to dislocations at atomic scale, are not considered in this study, since they are of less importance for the material's strength. Moreover, the measurement resolution of most test methods is not small enough to measure type II and type III residual stresses.

Residual stresses are not always disadvantageous, e.g. glass plates are many times rapidly cooled to introduce compressive stress in the surface area of the plate. This the plate's overall loading resistance is increased and small cracks at the surface will not propagate easily into the plate. However, in most cases, residual stresses are unwanted, since they result in deformations from the intended shape. Moreover, tensile pre-stress adds to the stresses caused by external loading, thus reducing the strength of the parts and favoring propagation of cracks from the surface.

Each production process introduces some amount of residual stress [3]. However, the amount of residual stress that is introduced varies a lot among different production processes. Laser based processes (laser welding, Selective Laser Melting, etc.) are known to introduce large amounts of residual stress, due to the large thermal gradients which are inherently present in the processes. In case of laser bending, these stresses are e.g. used to deform sheet metal plates to a desired shape. Two mechanisms can be distinguished which cause residual stresses.

The first mechanism introducing residual stress is called the Temperature Gradient Mechanism (TGM, see Figure 1). It results from the large thermal gradients that occur

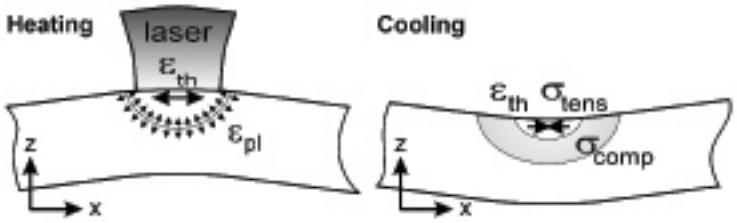

Figure 1: Temperature Gradient Mechanism inducing residual stress

around the laser spot. The TGM mechanism is commonly used for laser bending of sheets along straight lines. Due to the rapid heating of the upper surface by the laser beam and the rather slow heat conduction, a steep temperature gradient develops. The material strength simultaneously reduces due to a raise of temperature. Since the expansion of the heated top layer is restricted by the underlying material, elastic compressive strains are induced. When the materials yield strength is reached, the top layer will be plastically compressed. In absence of mechanical constraints, a counter bending away from the laser

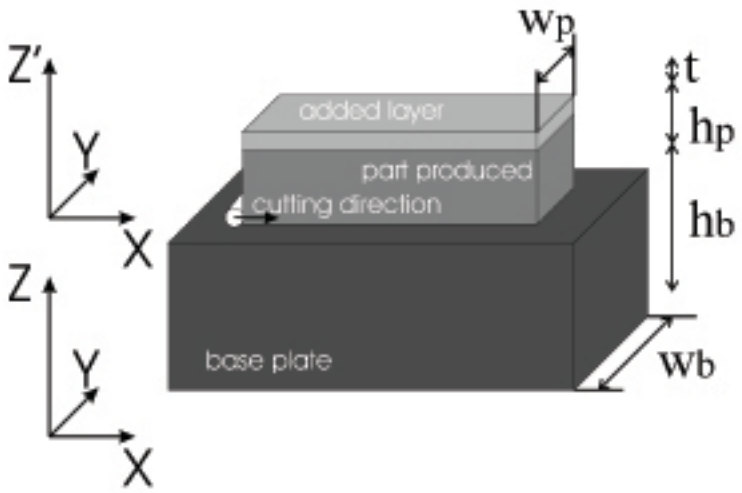

Figure 2: Simplified theoretical model of the SLM process

beam would be perceived. During cooling the plastically compressed upper layers start shrinking and a bending angle towards the laser beam develops. This mechanism is also present in SLS and SLM, where the underlying layers inhibit the expansion of the heated top layers. It is important to notice that this mechanism does not require the material to be molten.

A second mechanism that induced residual stresses is the cool-down phase of the molten top layers (in SLM). The latter tend to shrink due to the thermal contraction. This deformation is again inhibited by the underlying material, thus introducing tensile stress in the added top layer.

Simplified theoretical model

To get an idea of the residual stress profiles that would be found in Selective Laser Melting samples, a simplified theoretical model was developed. Assume that a part is being built on top of a base plate with height h_b. The part that was built so far has height h_p and the layer thickness is t (see figure 2). This simple theoretical model assumes that

- The base plate and the part being build are at room temperature
- The upper layer induces stress due to its shrinkage ($\alpha\Delta T$); the tensile stress is equal to the material's yield strength
- The stress σ_{xx} is independent of the y coordinate; the variation of the normal stress across the part's width is neglected
- The general bar theory is valid
- No external forces are applied to the combination part-base plate

At each moment, the equilibria of force (eq. 1) and momentum (eq. 2) need to be obeyed, since there are no external forces acting on the system.

$$\int \sigma_{xx}(z)dz = 0 \tag{1}$$

$$\int \sigma_{xx}(z) z dz = 0 \tag{2}$$

Due to the continuity of the deformation at the border between the base plate, following strain profile is asumed over the combination base plate - part:

$$\epsilon_{xx}(z) = az + b \tag{3}$$

Due to the different stiffness of the base plate and the part material, this deformation results in different stress levels; the stress profile reveals a jump at the border between the base plate and the part. Suppose that m represents the ratio of base plate stiffness to the part's stiffness:

$$m = \frac{E_{base}}{E_{part}} \tag{4}$$

Using this assumption, the equilibrium conditions can be rewritten as:

$$\int_0^{h_b} m(az+b)\, dz \; + \int_{h_b}^{h_b+h_p} (az+b)\, dz \; + \int_{h_b+h_p}^{h_b+h_p+t} \overline{\sigma}\, dz \; = 0 \tag{5}$$

$$\int_0^{h_b} m(az+b) z\, dz \; + \int_{h_b}^{h_b+h_p} (az+b) z\, dz \; + \int_{h_b+h_p}^{h_b+h_p+t} \overline{\sigma} z\, dz \; = 0 \tag{6}$$

From equations 5 and 6, the coefficients a and b can be derived:

$$a = -6\, \overline{\sigma}\, t\, \frac{\left(2mh_b h_p + mh_b h_p t + h_p^2 + h_p t + mh_b^2\right)}{\left(4mh_b^3 h_p + h_p^4 + m^2 h_b^4 + 6mh_b^2 h_s^2 + 4mh_b h_p^3\right)} \tag{7}$$

$$b = \overline{\sigma}\, t\, \frac{\left(2mh_b^3 + 6h_p mh_b^2 + 3mh_b^2 t + 6h_b h_p^2 + 6h_b h_p t + 2h_p^3 + 3h_p^2 t\right)}{\left(4mh_b^3 h_p + h_p^4 + m^2 h_b^4 + 6mh_b^2 h_s^2 + 4mh_b h_p^3\right)} \tag{8}$$

Equations 5 and 6 assume that the part and the base plate are equally wide. Usually the base plate is wider than the part. Including the widths of the part and the base plate in the equations would result in a different m factor: $m = \frac{E_{base} w_{base}}{E_{part} w_{part}}$. The influence of a wider base plate can thus be simulated by increasing the E modulus of the base plate.

After the production, the parts produced are generally removed from the base plate. To simulate this, a relaxation stress must be added to the stress profile calculated in the part. This relaxation stress has a linear profile:

$$\sigma_{relaxation}(z') = cz' + d \tag{9}$$

The constant part of the relaxation stress corresponds to a uniform shrinkage of the part that is being removed from the base plate. The linear part results in a curvature of the part. The coefficients c and d can be determined by recalculating the equilibrium conditions for the produced part:

$$c = -6\, \frac{-2\int_0^{h_c} z'\sigma(z')dz' + h_c \int_0^{h_c} \sigma(z')dz'}{h_c^3} \tag{10}$$

$$c = 2h_c\, \frac{\int_0^{h_c} \sigma(z')dz' - 3h_c \int_0^{h_c} z'\sigma(z')dz'}{h_c^2} \tag{11}$$

Theoretical residual stress profiles

When a layer is added to the base plate, it induces a compressive stress in the upper part of the base plate and a tensile stress in the lower part. When successive layers are added on top, each layer induces a certain stress profile in the base plate, but also in the underlying solidified layers, thus reducing the initial tensile stress present in these layers.

Figure 3 shows the resulting stress profile in the part and baseplate, after 50 layers (properties: $E_{base} = 210$ GPa, $E_{part} = 110$ GPa, $t = 50\mu m$, $\overline{\sigma} = 300$ MPa). It can be seen that the stress at the last added layer equals the yield stress of the material.

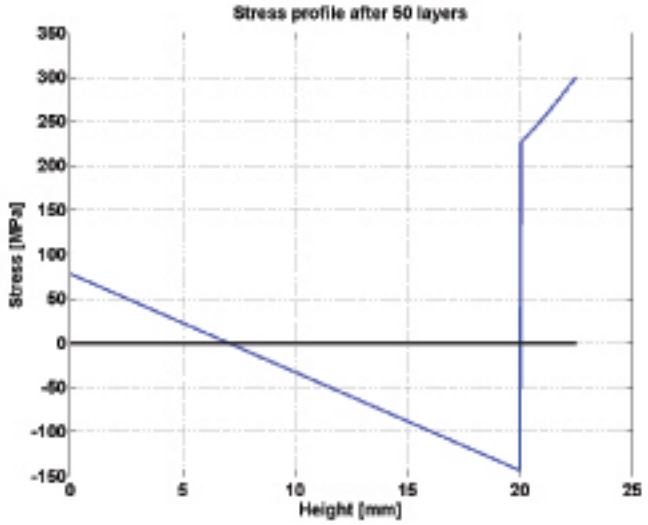

Figure 3: Residual stress in the part and the base plate

When the part is removed from the base plate, the stress state in the part is drastically changed; due to the relaxation, the resulting stress in the part will be much lower. The constant part of the relaxation stress corresponds to the shrinkage of the part, whereas the linear part of the relaxation stress corresponds to the bending of the part. Figure 4 shows the relaxation principle and the resulting stress in the part.

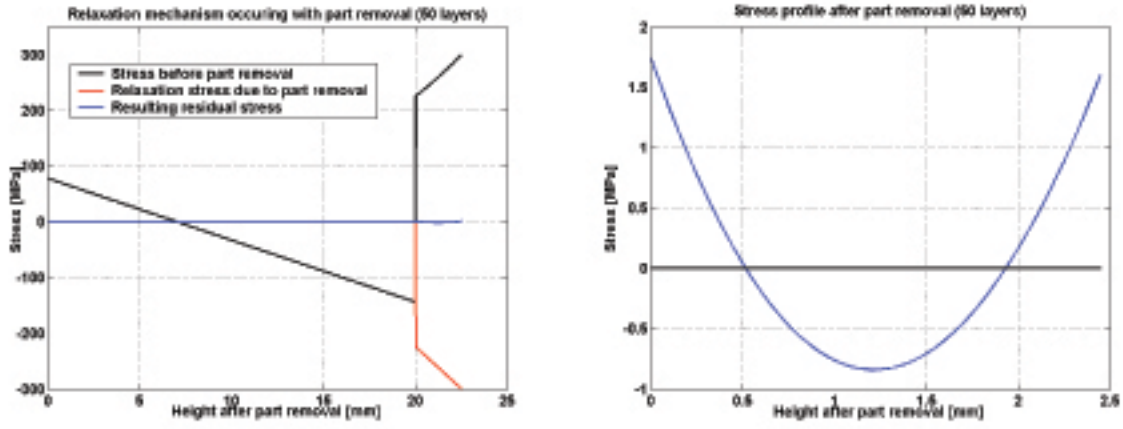

Figure 4: Relaxation of the residual stress and resulting stress in the part

Influence of number of layers, base plate geometry and material properties

Number of layers

Figure 5 shows the influence of the number of layers on the residual stress profile. Before

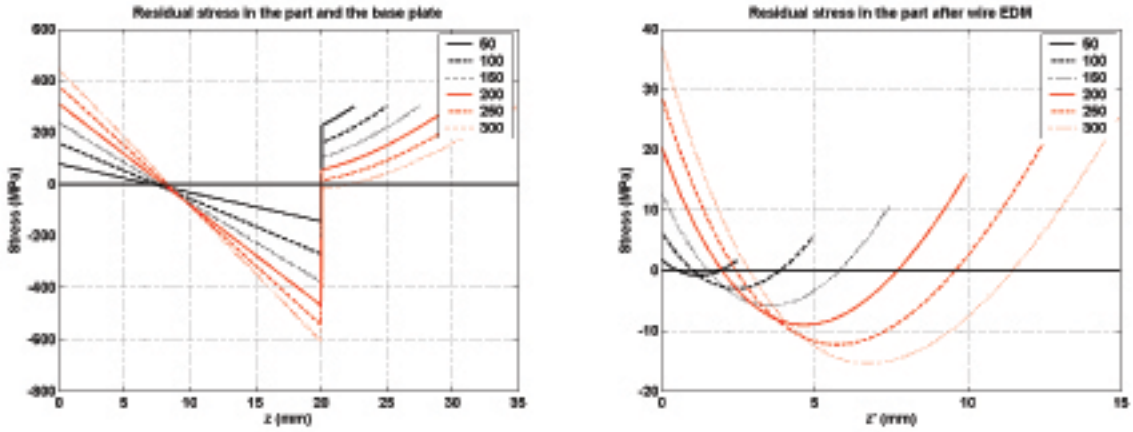

Figure 5: Influence of the number of layers on the residual stress profile

part removal, the stress in the part equals the yield strength at the top. However, when the number of layers keeps increasing, compressive stresses occur at the bottom of the part. It can also be seen that the stresses in the base plate become very large, so plastic deformation of the base plate could occur. However, this behavior is not included in the model. After part removal, a more or less symmetrical stress profile remains in the part. At the top and bottom of the part, tensile residual stress remains, in between, there is a zone of compressive stress. The tensile residual stress is somewhat larger at the bottom than at the top surface.

Figure 6 shows the influence of the number of layers on the relaxation stresses. It

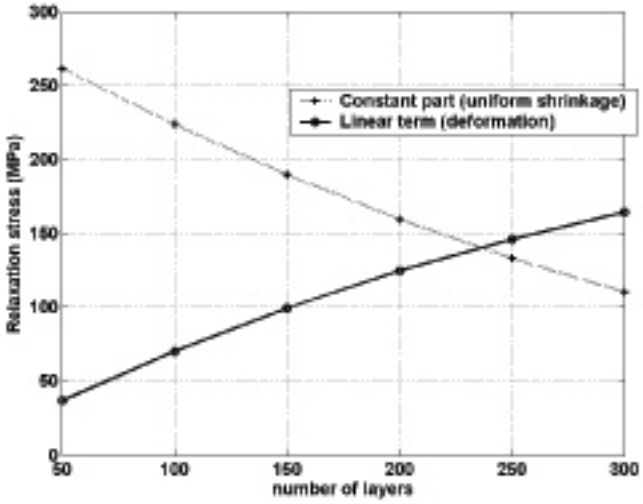

Figure 6: Influence of the number of layers on the relaxation stress

can be seen that the constant part, which corresponds to the shrinkage in x direction,

is reduced by adding more layers. However, the linear part is increased. However, one should not conclude that this would increase the part's bending deformation, since the surface moment of inertia increases also with the number of layers (according to h^3).

Base plate geometry

Since the model assumes that the general bar bending theory is valid, the width of the base plate can be combined with its E modulus to represent the stiffness. The base plate height, however, must be treated separately. Figure 7 shows the influence of the base plate height on the stress profiles. According to this simple theoretical model, the height

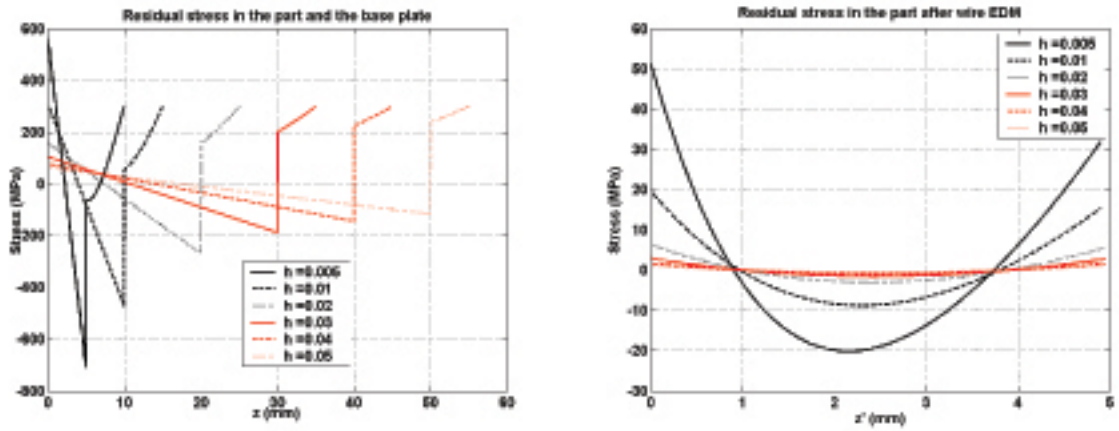

Figure 7: Influence of the base plate height on the residual stress profile

of the base plate has a clear influence on the residual stress distribution. Before part removal, a higher height results in a lower stress level in the base plate itself and a more uniform stress level in the part. This means that a thick base plate results in a smaller deformation due to part removal, compared to a thin base plate. Since almost all stress is released by a uniform shrinkage, only little residual stress remains in the part after removal. Figure 8 shows the influence of the base plate height on the relaxation stress components.

Material properties

Figure 9 shows the influence of the material's yield strength on the residual stress being developed. The higher the yield strength, the higher the stresses being developed. The stresses after part removal are also larger. However, the higher residual stresses are compensated by the increased strength of the part.

Conclusions

- Stress profiles before removal consist of a large zone of tensile stress at the upper zone of the part being build. The maximum stress is reached at the surface of the part (equals the yield stress). The stress reduces with decreasing z values. The lower part of the base plate is under tensile stress, the upper part in under compressive stress.

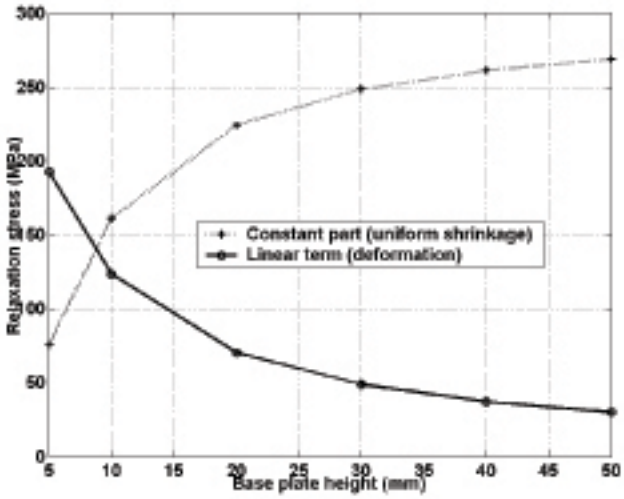

Figure 8: Influence of the base plate height on the relaxation stress components

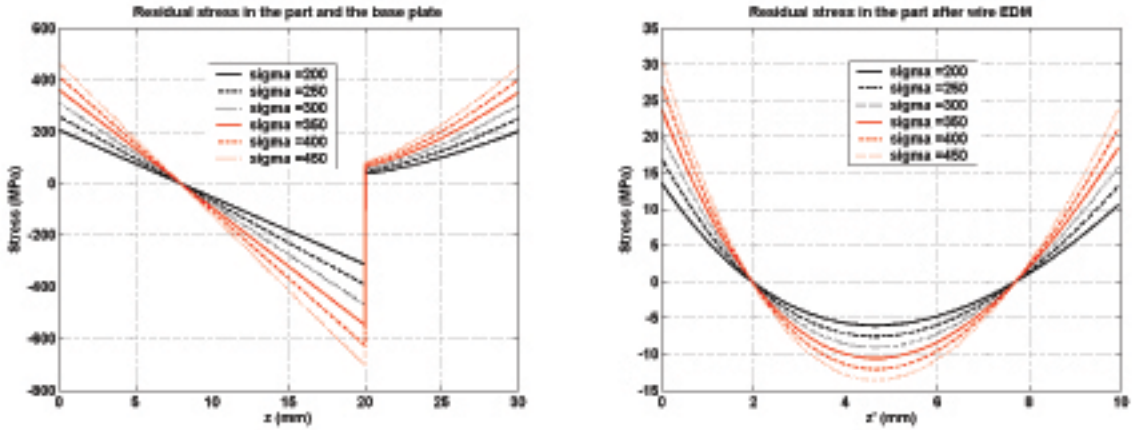

Figure 9: Influence of the materials yield strength on the residual stress profile

- Part removal drastically reduces the residual stresses which are present in the part; the residual stress relaxes by a uniform shrinkage and a bending deformation. The residual stress after removal consists of a zone of tensile stress at the upper and lower zone of the part and a compressive stress zone in between. The stresses after part removal are much smaller than before part removal.
- The more layers are added, the larger the final residual stress will be. The shrinkage along the x axis will reduce when the amount of layers increases.
- The higher the base plate, the smaller the resulting residual stresses will be (for a fixed part height). A very high base plate results in a large shrinkage in x directing, while the bending deformation becomes smaller. A small base plate height results in high residual stresses in the part and in a high bending deformation.
- The higher the yield strength of the added material, the higher the resulting residual stresses.

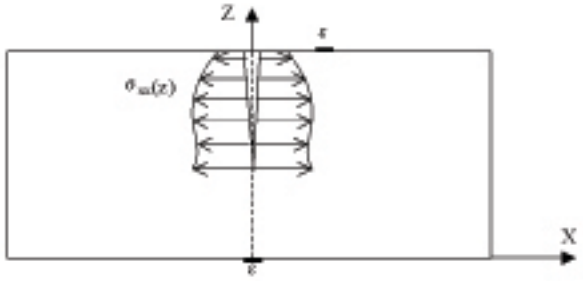

Figure 10: Schematic representation of test sample

Experimental measurement of residual stress: the Crack Compliance Method

In order to measure the residual stresses in the parts, a novel experimental model is used, based on measurement of the part's deformation when the stresses are relieved. The method is called the 'Crack Compliance Method' (CCM)[4, 5]. Compared with 'traditional' test methods like X-ray diffraction or hole drilling, this method has the advantage that trough-thickness measurements can be preformed in a simple and cheap way [6]. The method will be shortly explained first, without discussing the mathematical implementation in detail.

Figure 10 shows a sample in which an unknown residual stress distribution $\sigma_{xx}(z)$ is present. This stress distribution is supposed to be independent from the y coordinate. One ore more strain gauges are connected to the sample's surface at known positions. Next, the part is cut in subsequent small steps using wire Electric Discharge Machining (EDM). After each cutting step, the strain is measured at each strain gauge position.

Suppose that the unknown stress distribution can be written as a series expansion of functions $P_j(z)$.

$$\sigma_{xx}(z) = \sum_{j=1}^{n} A_j P_j(z) = [P]\{A\} \tag{12}$$

The set of basic functions $P_j(z)$ can be polynomials, Fourier series, etc. Legendre polynomials are generally chosen, since these polynomials (from order 2 on) automatically obey the equilibrium conditions of force and momentum. For each basic function $P_j(z)$ we can now calculate the strain profiles that would be measured at the strain gauge locations, if this basic function would be the actual residual stress profile. These calculations are generally preformed using a Finite Element method [1]. The calculated strains, belonging to each of the basic functions, are referred to as 'compliances' $C_j(d_i)$. Using the superposition principle, the total strain due to the sum of all the basic functions can be written as:

$$\epsilon_{xx}(z) = \sum_{j=1}^{n} A_j C_j(z) = [C]\{A\} \tag{13}$$

From equation 13, the coefficients A_j can be calculated using a least-squares fitting algorithm:

$$\{A\} = ([C^T] \cdot [C])^{-1} \cdot [C]^T \cdot \{\epsilon_{measured}\} \tag{14}$$

[1] The calculations were preformed using the Abaqus FEM package

Substitution of the coefficients $[A]$ in equation 12 results in the residual stress profile.

Figure 11 shows the compliance functions that were calculated for the selected top face and back face strain gauge positions.

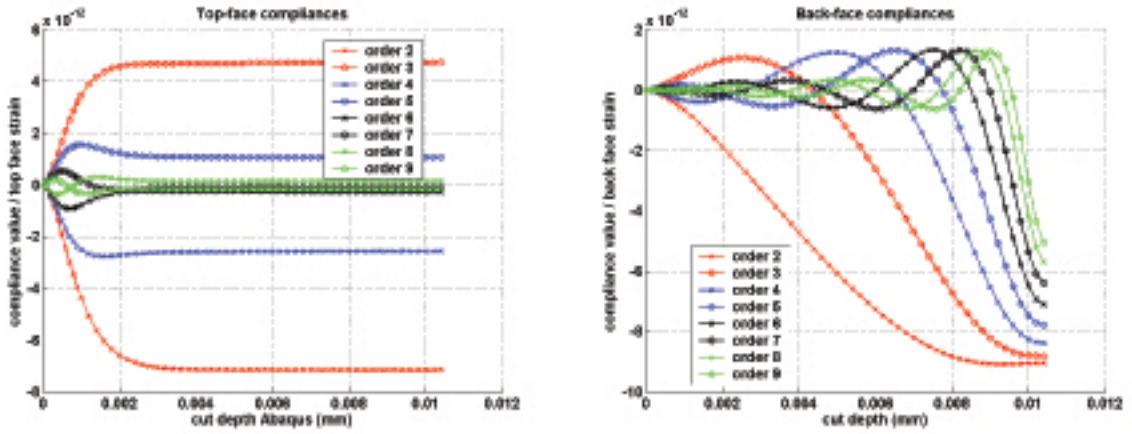

Figure 11: Top face (left) and back face (right) Compliance functions for 2nd - 9th order Legendre polynomials

In practise, the strains are measures at two locations, while the parts are being cut by wire-EDM. Figure 12 shows the practical setup.

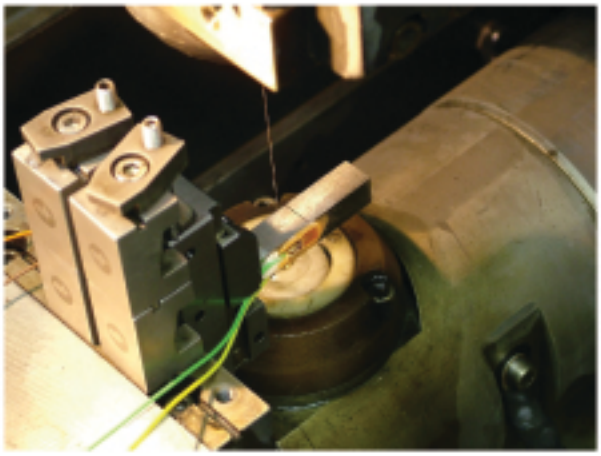

Figure 12: Practical setup of the CCM method

Experimental results

Test of the CCM method

In order to evaluate the suitability of the Crack Compliance method to do residual stress tests on SLM samples, and to check the FEM model being used, some initial experiments were preformed on samples with a know residual stress distribution.

A first tests preforms a stress measurement on an aluminium sample that was heated up to 200 degrees for 1 hour and cooled in air, to remove any residual stresses that might be inside the sample.

Figure 13 shows the stress distribution that was calculated from the strain measurements. As it can be seen, the stress level of 0 MPa lies within the two-sigma uncertainty bound (95% confidence limit) at most points.

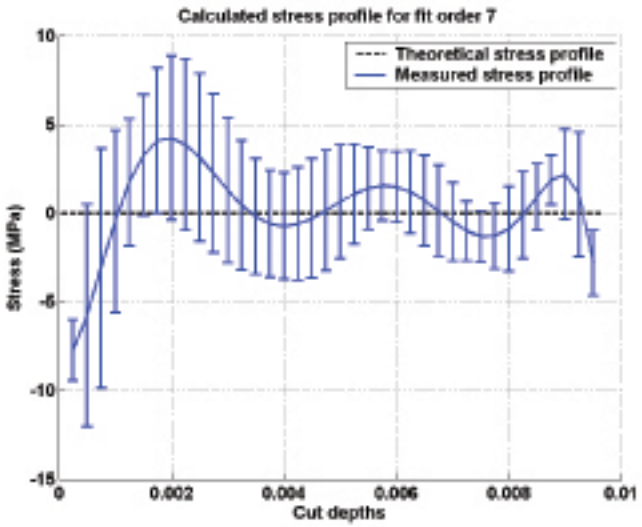

Figure 13: Calculated stress distribution in a stress free Al test sample

Using a four point bending setup some test samples were produced, having a known stress distribution. The four point bending test ensures a constant bending moment between the between the two middle contact points. The samples were bent until plastic deformation occurs at the upper and lower zones of the parts. After removing the force, a new equilibrium is formed, that can be calculated from the recorded force values and the yield strength. Figure 14 shows the calculated stress profile for one of the test samples. The stress distribution that is calculated this way, assumes that the samples are bent according to the general bar bending theory. It also assumes a perfect elastic-plastic behavior of the material, with a clear yield strength; in reality the real stress profile could be slightly different, but the general tendencies can be assumed to be correct.

Figure 15 shows the stress profile that is calculated from the measured strains. It can be seen that the calculated stress distribution matches the 'known' stress profile rather well. However, at some points large deviations occur.

Figure 16 shows the calculated stress distribution for a second test sample. In this case, the deviations are much larger. This is due to the steepness of the 'real' stress profile, which cannot be fit accurately with the set of Legendre polynomials that is being used. This is indicated in figure 17 which shows the optimal fit of the 'real' strain profile using the Legendre polynomials up to order 7. In order to fit these sharp peaks accurately, higher order polynomials are necessary.

When sharp peaks are expected in a residual stress profile, the Legendre polynomials are therefore not the ideal ones and other types of basic functions are favorable. However, from the theoretical model there is no reason to expect sharp peaks in the residual stress profiles, thus the Legendre polynomials with their inherent force and momentum equilibrium were used.

Description of test samples

Table 1 summarizes the most important test parameters of the test samples. All test

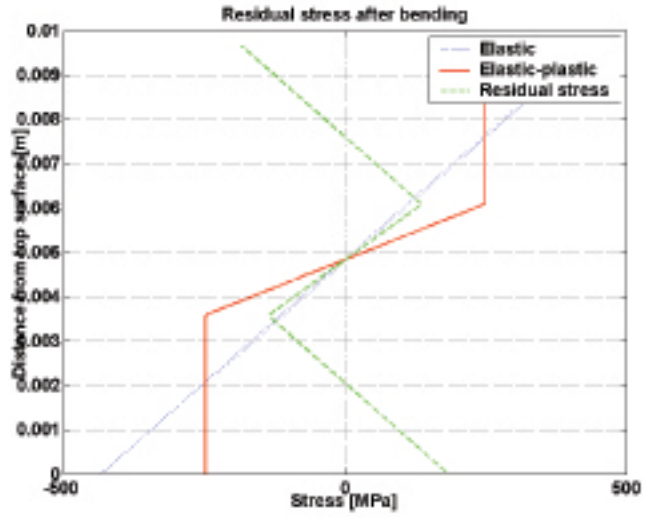

Figure 14: Calculated stress distribution in bent test sample 1

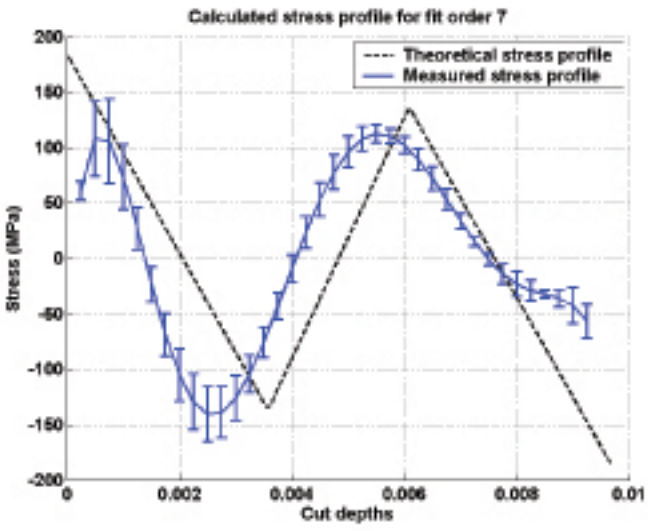

Figure 15: Calculated and measured stress distribution in bent test sample 1

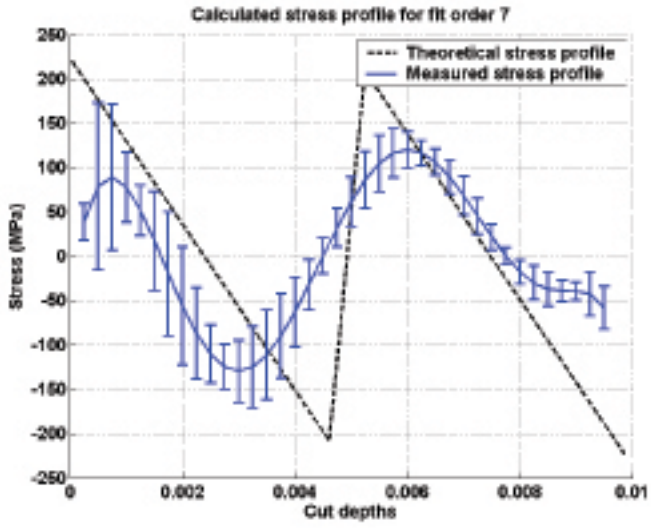

Figure 16: Calculated and measured stress distribution in bent test sample 1

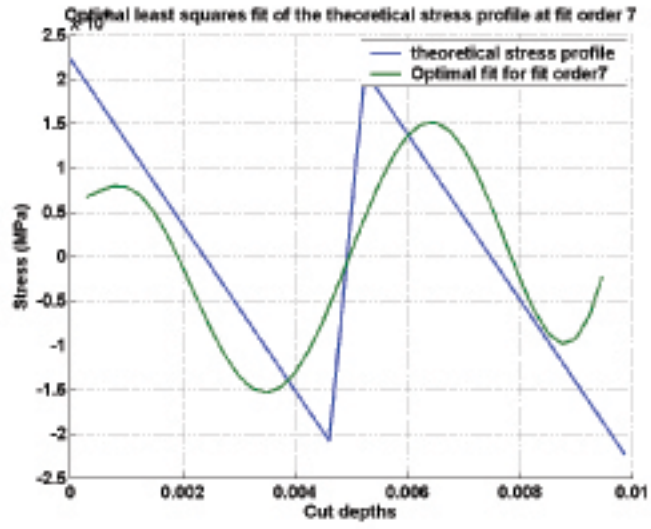

Figure 17: Calculated stress distribution in a stress free Al test sample

Length	50 mm
Width	10 mm
Height	10.5 mm
Laser power	100 W
Scanning speed	400 $\frac{mm}{s}$
Scan spacing	140 μm
Layer thickness	30 μm

Table 1: Parameters used for the production of all test samples

samples were produced from a standard stainless steel powder (grade 316L). The parts were built on top of a 15 mm thick stainless steel substrate plate.

Influence of the exposure strategy

The exposure strategy of the laser beam highly influences the thermal gradients which occur in the parts being produced. To test the influence of the exposure strategy on the residual stresses, a set of test samples was made using different scanning strategies. Figure 18 shows the different exposure strategies that were used.

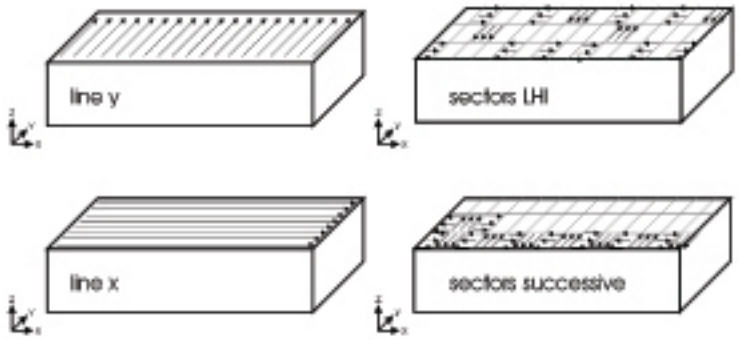

Figure 18: Different exposure strategies

The 'line Y' part is scanned along the Y axis and is thus also referred to as 'short track' scanning, while the 'line X' part will be named 'long track' scanning. To test the influence of the sector scanning, two different sector sizes were used: 5 by 5 mm and 10 by 10 mm. The position of the islands is shifted in X and Y direction between successive layers. The sector scanned parts discussed in this paragraph are all scanned according to a certain patented pattern, which minimizes the thermal influence of previous scanned sectors on the next scanned sector. The influence of the sector scanning order is investigated in the next paragraph.

Figure 19 shows the stress distributions that were measured for the exposure strategies. Some important conclusions can be derived:

- All stress profiles correspond to the general tendency of a small zone with high tensile stresses at the top of the part, followed by broad zone of compressive stress and again a small zone of tensile residual stress.
- There is a clear difference between 'short track' scanning and 'long track' scanning: scanning along the Y direction results in the largest values for σ_{xx}, while scanning along the X direction results in the smallest values.

- Division of the part surface in smaller sectors yields an intermediate stress level; the top layer stress lies between the stress resulting from 'long' and 'short' scanning of the whole part surface.
- There is no significant difference in the resulting stress profile between 5 and 10 mm sector size.

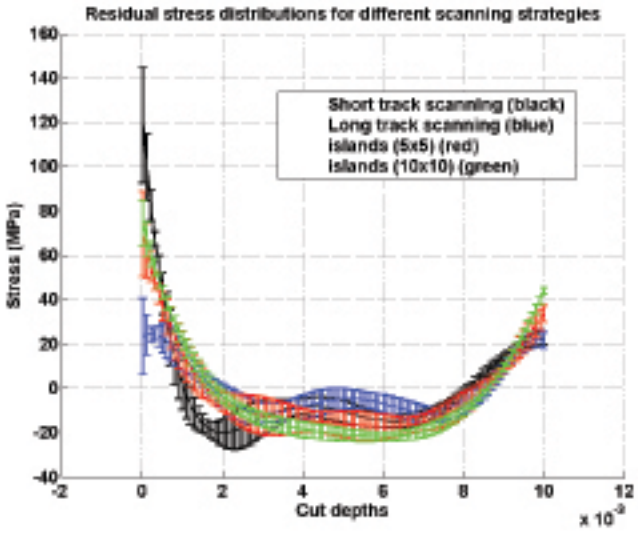

Figure 19: Measured stress distributions for different exposure strategies

A possible explanation for the reduction of the maximal stress level in case of sector scanning, is the fact that the stress at the borders of each individual sector - that has no neighbor sectors yet - is zero, since no material exhibits its contraction at the sector borders (see figure 20). When more sectors are added, neighboring sectors are connected and the stress level also rises at the sector borders. However, the overall stress level will be still be lower than than the maximum stress level in case of simple line scanning in the perpendicular direction.

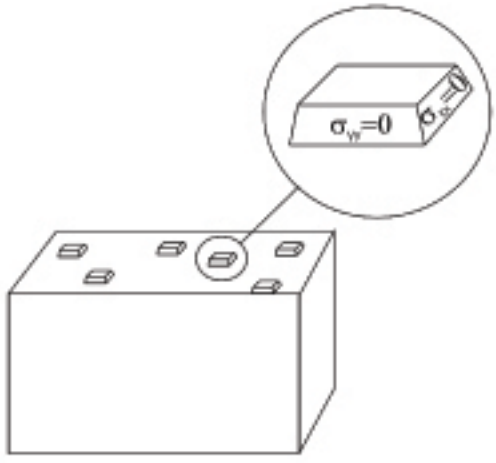

Figure 20: Sector scanning mechanism leading zero normal stress the first sector borders

Influence of the sector scanning order

We know now that a subdivision of the part surface can reduce the largest tensile stresses that occur in the upper layers of the parts being produced. However, the question remains how to exposure these sectors. There are number of ways to do so. Four different exposure orders were tested in the investigation, all with the same sector size (3 mm to 3 mm).

1. Scanning of the sectors along the width of the part
2. Scanning the sectors along the length of the part
3. Scanning the sectors in a randomized order, minimizing the mutual thermal influencing of the different sectors

Since the exposure order of the sector influences the thermal gradients that occur, it also affect the level of residual stress in the parts. Figure 21 shows the difference between the two first exposure orders. It can be seen that scanning the sectors along the width of the part (blue curve) yields a larger σ_{zz} value at the top of the part, than scanning along the part's length (red curve). This is no surprise, since the exposure order along the part width, corresponds to the 'short track' scanning strategy, if the sector size goes to zero. The stress level in case of the randomized scanning order, was comparable to the stress

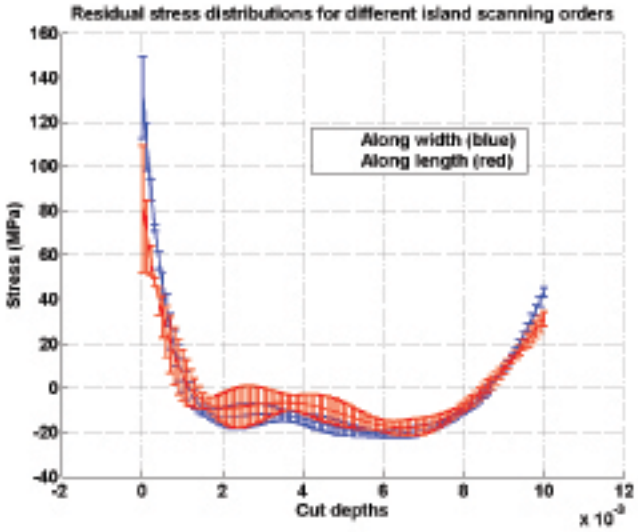

Figure 21: Measured stress distributions for different sector exposure orders

level, when scanning along the length of the part (red curve in figure 21), however, a bad top face reading resulted in a high uncertainty border.

Post scanning of the produced parts

To simulate an stress reduction heat treatment, post scanning of the part surface was investigated. After the normal exposure of each layer, the same layer was exposed again, at a lower energy level. Four parts were tested, with a post scanning energy of 10, 33, 50 and 100 % of the normal layer energy, by increasing the scan speed accordingly. Each of the parts was scanned with a 'short track' exposure strategy, as well for the normal scanning as the post scanning step. Figure 22 shows the measured stress distributions

for the 50 and 100 % post scanning levels, compared to the case without post scanning. It can clearly be seen that the 50% post scanning level reduces the tensile stress in the upper zone of the part (from 120 +/- 7 MPa to 84 +/- 11 MPa). Scanning each layer twice with the normal scanning parameters does not reduce the residual stresses inside the part; the already solidified layer is just remelted partially and the same residual stress distribution remains. The stress reducing effect of heating the underlying layers could result in a reduction of stress levels, but it is cancelled out by the TGM mechanism (see paragraph) that introduces new stress inside the part.

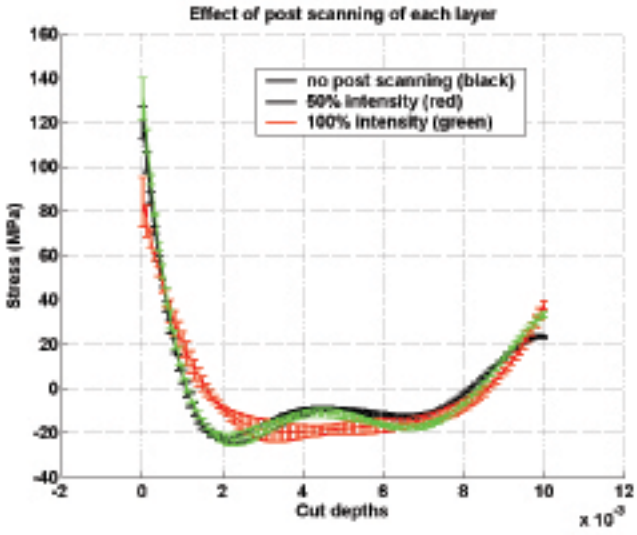

Figure 22: Measured stress distributions for different post-scanning parameters

X-ray diffraction experiments

The Crack Compliance method that was used in the experiments, offered the possibility to measure the residual stress trough the thickness of the test samples, unlike more traditional XRD and hole drilling stress measurement methods. Alas, the Crack Compliance method fails to measure the stress at the part surface accurately, because of several reasons, some of which were already mentioned before:

- The first useful data point is the strain value recorded at the first cut depth. Therefore the stress at the part surface is already an extrapolation of the calculated stress profile.
- The first few stress readings are rather small (less than 5 micron strain), and the uncertainty on these readings is therefore relatively large, resulting in a large stress uncertainty near the upper surface.
- The top face strain readings are very sensitive to the exact distance between the gauge and the edge of the cut.A slight positioning error of the top face gauge results in a large variation in the top face strains, causing erroneous results near the surface.

To cope with the large uncertainty of the stress readings near the surface, additional XRD tests were preformed on several SLM samples. Due so practical size limitations, the SLM

samples tested with the Crack Compliance Method, could not be tested using XRD, so a different set of test samples was produced.

The X-ray diffraction stress measurements were preformed on a Siemens D500 diffractometer. The diffraction peak of the 316L stainless steel material at a 2θ angle of 147 degrees was used to measure the peak shift.

Sample preparation

A first X-ray diffraction experiment on a untreated SLM sample, resulted in a stress level of 12 +/- 7 MPa. This unrealistically low value was caused by the roughness of the top surface. Since the X-rays penetrate the material only to a depth of about $30\mu m$, large roughness values prohibit a correct stress measurement.

To cope with this problem, an EDM finishing cut was used to remove the peaks from the surface. However, the EDM operation itself introduces large tensile stresses in a 40 μm thick zone below the surface [7], which deteriorates the measurement result. Therefore, the thermally influenced layer from the EDM operation was removed by chemically etching a small top layer from the samples[2].

Figure 23 shows the sample preparation steps schematically. Figure 24 shows the

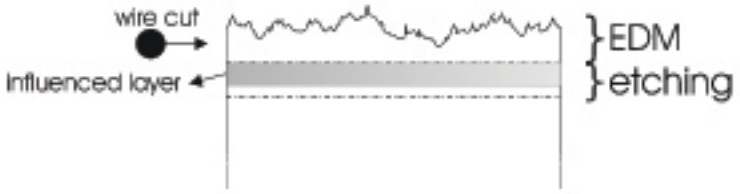

Figure 23: XRD sample preparation steps

results of three different XRD measurement on a stress free dummy sample that was used to check the influence of the sample preparation steps.

The first XRD measurement indicates a low but non-zero stress value in X direction (the Y direction was not measured). The non-zero value was probably caused by a small oxidation layer that resulted from the heat treatment. Next, the dummy sample was cut with wire-EDM on a finishing regime. The second XRD measurement reveals indeed very large stress values X and Y direction. There is no significant difference between the direction of the cut and the direction of the wire. The third XRD measurement indicated the stress values after the etching step. It is clear that the small thermally influence layer of the EDM process is removed in the etching step and a zero stress value is measured indeed in X and Y direction.

Due to the removal of the upper layer, the stress values that are measured are not any more the values at the upper layer of the part. However, the total removed thickness of about $120\mu m$ is small enough compared to the total height of the XRD test samples (10.5 mm) to consider them as the top layer stress values.

The influence of the base plate removal step is shown in figure 25. The sample that was tested was exposed with a random sector exposure. Thus, the stresses are equally large in X and Y direction. The same sample was then cut from its base plate and the stresses were measured again. It is clear that the base plate removal yields a large reduction of the stress levels.

[2]A mixture of HCl and HNO_3 was used to remove a top layer of +/- $80\mu m$ thickness from the top surface

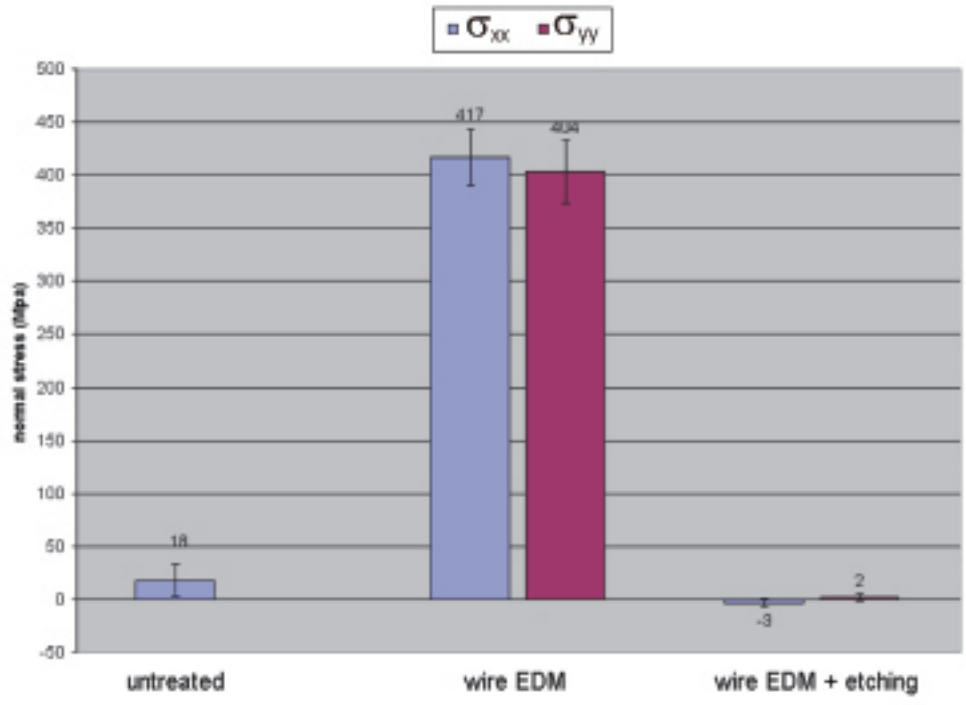

Figure 24: XRD result with stress free dummy sample

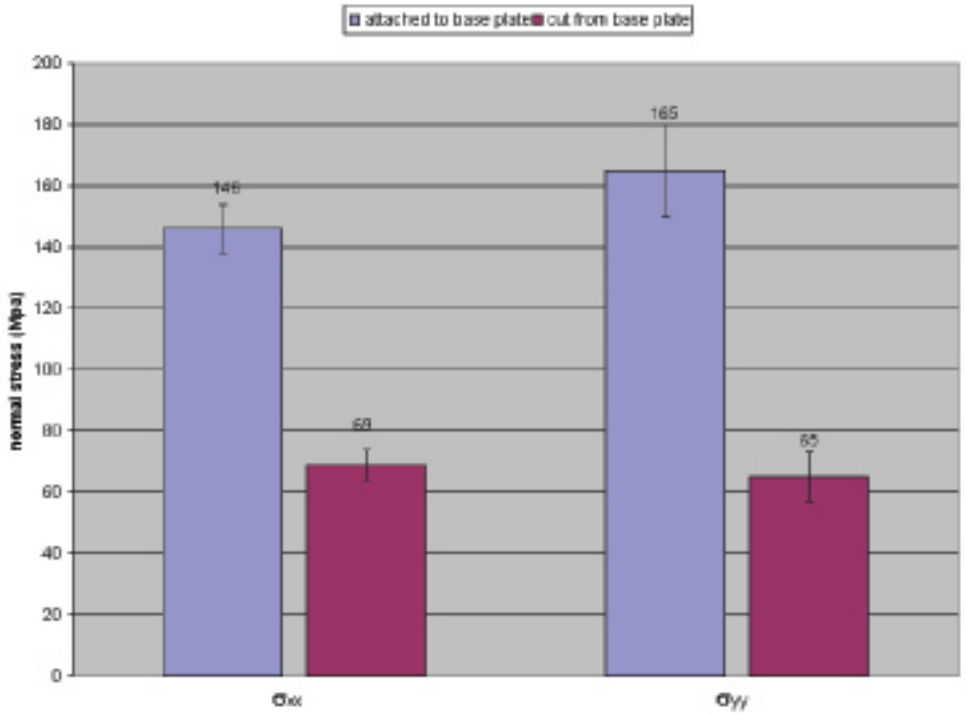

Figure 25: influence of base plate removal

The influence of the number of layers was investigated by testing a series of three samples, having a height of 2.5, 5 and 10 mm respectively. The base plate was removed with all samples. All three samples were scanned without dividing the surface in sectors, to check the influence of the scanning direction on the residual stresses. Figure 26 shows the axis orientation and the exposure strategy that was used. From figure 27 it can

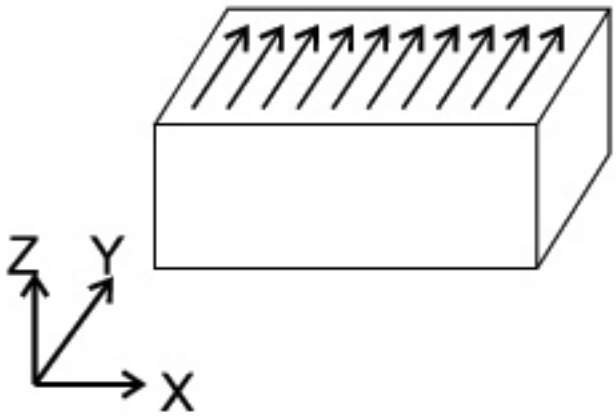

Figure 26: Exposure strategy and axis orientation

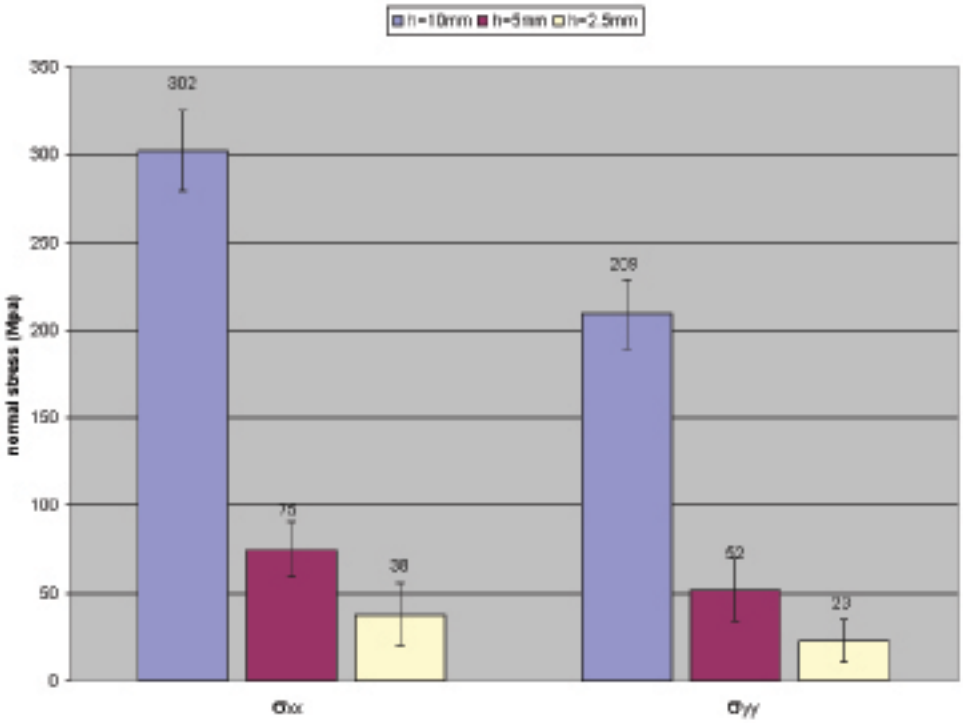

Figure 27: influence of the sample height

clearly be seen that the sample height has a large influence on the residual stress level, as expected from the theoretical model. Furthermore, figure 27 reveals the influence of the scanning direction on the residual stresses; the stresses perpendicular to the scanning direction are significantly larger than the stresses along the scanning direction. This result corresponds to the Crack Compliance experiments.

Since residual stresses arise from temperature gradients, heating up the build platform can reduce the stress levels present in the parts [8]. To validate this assumption the build platform was heated up to 200 degrees. Figure 28 shows the effect of the raised based plate temperature. It is clear that the stresses are reduced by the base plate heating. However, the stress reduction is rather poor. It can be expected that a higher base plate heating temperature will result in a greater stress reduction. Like figure 27, figure 28 also clearly indicates the influence of the scanning direction.

In general, there is a good qualitative agreement between the theoretical model, the

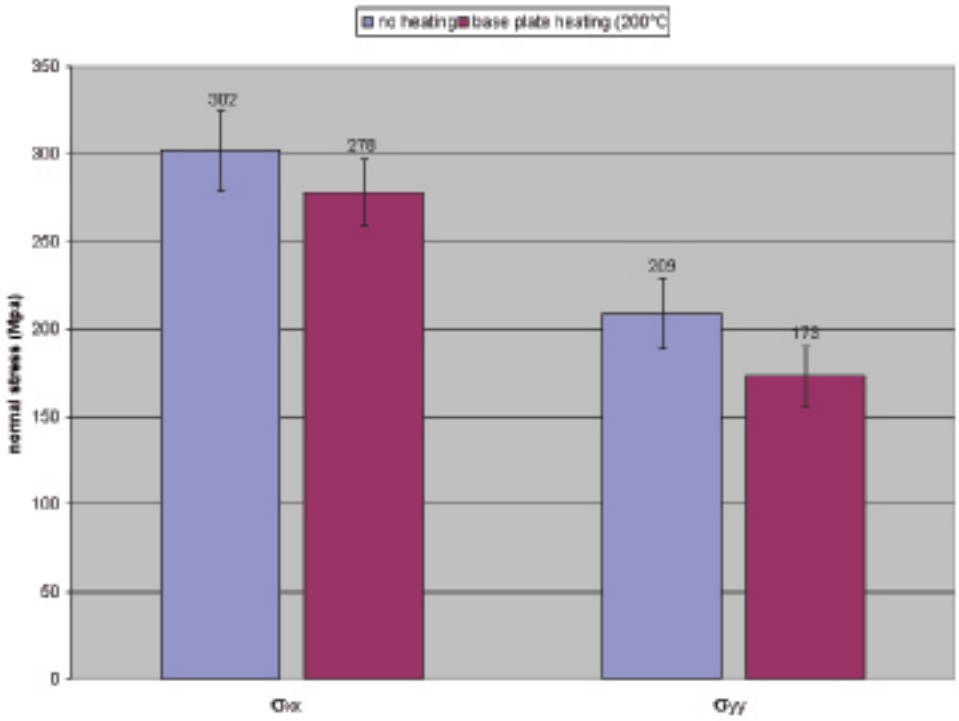

Figure 28: influence of base plate heating

Crack Compliance experiments and the XRD tests. However, a quantitative comparison is not easy, because of several reasons:

- The theoretical model calculates the stresses resulting from the shrinkage of the added molten layers. It does not include the Temperature Gradient Mechanism, which induces extra residual stresses.
- The sample geometry of the Crack Compliance test samples and the XRD samples was different, due to practical reasons.
- The Crack Compliance test samples and the first batch of XRD test samples, used non optimized scanning parameters, which appeared to contain a high degree of porosity. This resulted in stress values much lower than in the case of full density, since the stress equals zero at each porosity border. The XRD samples from figures 27 and 28 were build with optimized scanning parameters, yielding nearly 100% density and having much higher stress values.

Conclusions

This paper presented a theoretical and experimental investigation on residual stresses in Selective Laser Sintering and Selective Laser Melting. A simple theoretical model could predict the basic shape of the residual stress profile of a basic rectangular geometry. Two experimental methods - the Crack Compliance Method and an X-ray diffraction method - were used to validate the theoretical predictions and to find a qualitative and quantitative estimation of the residual stresses.

From the theoretical model and the experiments, some important conclusions can be derived:

- A distinction should be made between parts that remain connected to the base plate and parts that are removed afterwards. In general, parts that stay connected to the baseplate contain very high stress levels, in the range of the material's yield strength. Parts that are removed from the base plate, contain much lower stress levels, but they suffer from deformation during part removal.
- The basic residual stress distribution in the Z direction for a part removed from its base plate, consists of a zone of tensile stresses just below the upper surface, followed by a large zone of compressive stress, to end again with a tensile stress zone at the bottom. The magnitude of the stresses depends amongst others on the part height and the stiffness and height of the base plate.
- The exposure strategy that is being used to fuse the powder layers, has a large influence on the residual stress levels being developed. In general, the stresses are larger perpendicular to the scan direction than along the scan direction. A subdivision of the surface in smaller parts results in a lower maximum stress value and in equally large stresses in X and Y direction.
- It is possible to reduce the stress level by applying a heat treatment using the laser source. However, no drastic reductions could be obtained in this investigation.
- Heating of the substrate plate results in a reduction of the residual stress level, since temperature gradients are reduced.

Acknowledgements

This research was funded by the IAP project P5-08 of the Belgian Federal Science Policy and the GOA/2002/06 project from K.U.Leuven.

References

[1] J.P. Kruth, L. Froyen, M. Rombouts, J. Van Vaerenbergh, and P. Mercelis. New ferro powder for selective laser sintering of dense parts. In *Annals of the CIRP*, pages 139–142, 2003.

[2] J.P. Kruth, P. Mercelis, L. Froyen, and M. Rombouts. Binding mechanisms in selective laser sintering and selective laser melting. In *Proceedings of the Solid Freeform Fabrication Symposium*, pages 44–59, 2004.

[3] P.J. Withers and H.K.D.H. Bhadeshia. Residual stress, part 2 - nature and origin. *Materials Science and Technology, Vol. 17*, Vol. 17:366–375, 2001.

[4] M.B. Prime. Residual stress measurement by seccessive extension of a slot: the crack compliance method. *Applied Machanics Reviews*, Vol. 52/2:75–96, 1999.

[5] D. Nowell, D.A. Hills, and S. Tochilin. Use of the crack compliance method for the measurement of residual stress. In *Proceedings of the 6th International Conference on Residual Stresses, Vol. 2*, pages 845–852, 2000.

[6] H.J. Schindler. Residuals stress measurements in cracked components: capabilities and limitations of the cut compliance method. *Materials Science Forum*, Vols. 347-349:150–155, 2000.

[7] J.P. Kruth and Ph. Bleys. Measuring residual stress caused by wire edm of tool steel. *International Journal of Electrical Machining*, Vol. 5:23–28, 2000.

[8] Ch. Over. *Generative Fertigung von Bauteilen aus Werkzeugstahl X38CrMoV5-1 und Titan TiAl6V4 mit Selective Laser Melting*. PhD thesis, RWTH Aachen, 2003.